CRYSTALLOGRAPHY REPORTS, 2025, Vol. 70, No. 1, pp. 27–33

LATTICE DYNAMICS AND PHASE TRANSITIONS

PHASE TRANSITIONS IN POLY(VINYLIDENE FLUORIDE)-BASED COMPOSITE UNDER MECHANICAL STRESSES

© 2025 P. A. Vorontsov[a,*], V. D. Salnikov[a], V. V. Savin[a], S. A. Vorontsov[a], L. V. Panina[a,b], P. A. Ershov[a], and V. V. Rodionova[a]

[a] *Kant Baltic Federal University, Kaliningrad, Russia*
[b] *National University of Science and Technology "MISIS", Moscow, Russia*
**e-mail: pavorontsov@kantiana.ru*

Received November 25, 2024
Revised November 29, 2024
Accepted November 29, 2024

Abstract. In this work the phase transition in composites based on polyvinylidene fluoride and cobalt ferrite nanoparticles under uniaxial stretching at 100%, 200% and 300% is investigated. It was found that when the composite is stretched at 300%, there is a maximum increase in the β-phase fraction from 1% for the unstretched sample to 91%, while the electroactive phase increases from 74% to 92%. It was also found that tensile stretching of the composites leads to an increase in tensile strength: from 5.7 MPa to 85.0 MPa. This tensile pattern also contributes to an increase in coercivity, which is due to the increase in the interparticle distance in the composite structure. These results emphasise the importance of mechanical properties and phase changes in polymer composites containing ferrites for their future applications.

DOI: 10.31857/S00234761250104e3

INTRODUCTION

Polyvinylidene fluoride (PVDF) is a widely used polymer known for its thermal stability, chemical resistance, ferroelectric, pyroelectric and piezoelectric properties [1–3]. These properties make PVDF suitable for various applications such as sensors [4], energy harvesting devices [5] and biomedical applications [6].

The unique properties of PVDF are related to its structure and phase composition. It can exist in four crystalline forms (α, β, γ and δ), each of which arises from a different spatial arrangement of CH_2 and CF_2 groups [7, 8]. The piezoelectric and ferroelectric properties, which are decisive for applications, are possessed by the β- and γ-phases, so the task arises of increasing them in the polymer.

Recently, methods for expanding the properties of PVDF by creating composite materials based on it have been studied. One of the most common approaches is the inclusion of magnetic nanoparticles (MNPs) in the polymer matrix to obtain materials with multiferroic properties [9], including magnetoelectric ones. Due to this combination of properties, together with flexibility and biocompatibility, PVDF composites have the potential for use in biomedicine as scaffolds for cell stimulation [10, 11].

The paper presents the results of a study of PVDF composite materials with cobalt ferrite $CoFe_2O_4$ nanoparticles. An important part of research on the creation of devices and materials based on PVDF and nanoparticles is the enhancement of the magnetoelectric effect. One of the strategies for its increase is the enhancement of the piezoactive component of the composite by increasing the content of the β-phase. A number of techniques have been developed for the creation and processing of PVDF films with an increased content of the β-phase, such as obtaining films by electrospinning [12, 13], annealing, polarization, mechanical rolling, and their combinations [14]. In [14], it was possible to achieve 85% content of the β-phase in the PVDF film as a result of mechanical rolling, which turned out to be the best result in comparison with annealing and polarization.

The increase of the β-phase can be achieved by mechanical deformation of the polymer matrix, for example, by stretching [15]. However, to achieve the best result of the phase transition, it is necessary to select conditions that ensure the maximum transition from the α- and γ-phases to the β-phase. By studying the relationship between the degree of stretching of the composite and the formation of the β-phase, more effective materials can be developed. In this work, the effect of the degree of stretching of the PVDF-$CoFe_2O_4$ composite film at high temperature on the formation of the β-phase and on the change in crystallinity and tensile strength is studied.

METHODS AND MATERIALS

Materials. Polyvinylidene fluoride (m.w. 534 000, Sigma-Aldrich) in the form of a white powder, N, N-dimethylformamide (chemically pure, EKOS,

Moscow) were used for the preparation of the nanocomposite. $Co(NO_3)_2$ $6H_2O$ (⩾98%; LenReaktiv, St. Petersburg, Russia), $Fe(NO_3)_3$ $9H_2O$ (⩾98%; LenReaktiv, St. Petersburg, Russia), NaOH (⩾98%; LenReaktiv, St. Petersburg, Russia), distilled water (dH_2O) were used for the synthesis and modification of the surface of nanoparticles.

Fabrication of Oleic Acid Coated $CoFe_2O_4$ Nanoparticles. Magnetic nanoparticles were synthesized by the hydrothermal method described in detail in [16] with minor modifications. Cobalt nitrate (6.8 mmol) was dissolved in 32 ml dH_2O on a magnetic stirrer at 50ºC. Then iron nitrate (13.6 mmol) was added and complete dissolution was waited for. To carry out the coprecipitation reaction, sodium hydroxide 130.7 mmol in 48 ml dH_2O, preheated to 50ºC, was added. After that, the solution was placed in an autoclave (filled to 40% of the volume). The autoclave was heated to 200°C, the reaction took place for 12 h. The resulting powder was washed with water and ethanol, then dried. After drying, the particles were coated with oleic acid (OA) in the presence of tetrahydrofuran. After adding OA and tetrahydrofuran to the particles, the mixture was placed in an ultrasonic (US) bath until a stable colloid was formed, then kept at room temperature (20–22°C). After 2 h, $CoFe_2O_4$@OA was separated from the excess OA by centrifugation (30 min, 14,000 rpm) and dried. The method of drying to constant weight was used to determine the concentration of nanoparticles in the OA shell.

Coating of MNPs with oleic acid leads to better dispersion of nanoparticles in the polymer matrix due to the affinity of the terminal groups of OA to PVDF molecules, which leads to a decrease in the agglomeration of MNPs [17, 18]. Improving the distribution of MNPs in the polymer matrix is a promising approach to increasing the magnetoelectric response [17].

The X-ray diffraction pattern of the particles is shown in Fig. 1. The data for the coherent scattering region D_{XRD}, microstresses ε and lattice constant a, calculated using the Rietveld method, are presented in Table 1.

Manufacturing of nanocomposites. Composite films were obtained using the doctor blade method [19]. To prepare a PVDF solution, 1.8 g of powder was dissolved in 9.15 ml of N,N-dimethylformamide (DMF) at 45°C for 20 h. Cobalt ferrite ($CoFe_2O_4$@OA) weighing 0.25 g (10 wt. %, normalized to $CoFe_2O_4$) was broken up using an ultrasonic bath in 2.3 ml of DMF for 30 min until the solution became homogeneous. The resulting solutions were combined and mixed until homogeneous for 90 min at 45°C, applied to a glass substrate and uniformly distributed using a doctor blade with a given thickness (45 ± 2 μm). Then the glass substrate with the solution was placed in a drying oven for 20 h at a temperature of 65°C. After drying, the resulting film was divided into equal pieces, which were stretched by 100, 200 and 300% (Fig. 1) at 100°C. Stretching the composite by 400% led to rupture of the sample. The samples are designated as *S*0, *S*100, *S*200 and *S*300, where the number indicates the degree of stretching.

Study of magnetic properties of nanoparticles and composites. The measured magnetic properties of coated and uncoated nanoparticles and composites are presented in Table 1. The field dependences of magnetization for nanoparticles and composites with different degrees of stretching are shown in Fig. 2. The saturation magnetization values M_S for uncoated nanoparticles are close to the value for the bulk sample (82 vs. 88 emu/g) [20]. M_S for composites are consistent with the nominal magnetic core content for $CoFe_2O_4$@OA nanoparticles equal to 10% in the composite. The residual magnetization M_R/M_S for all samples was ~30–40%, which is lower than the expected value for

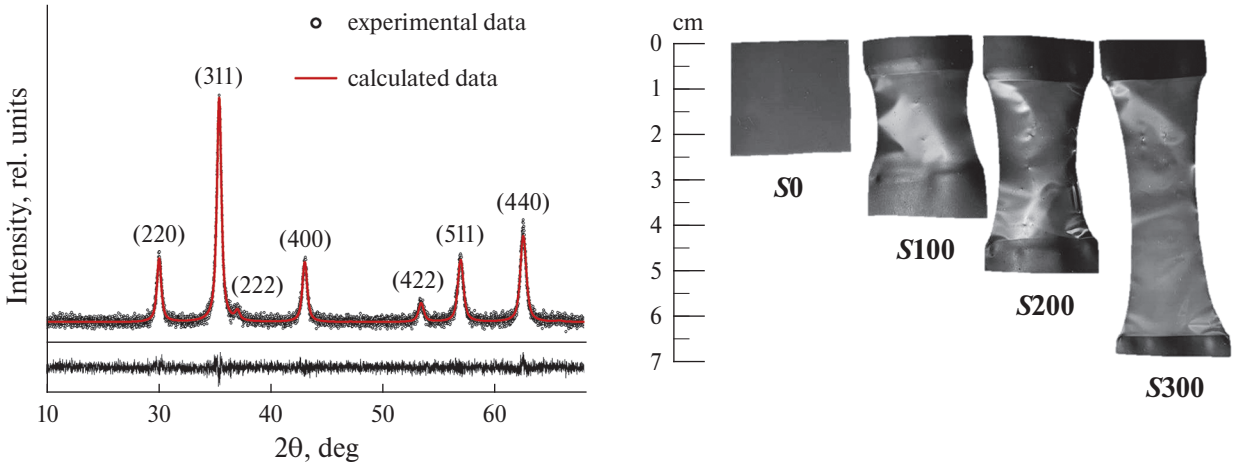

Fig. 1. X-ray diffraction pattern for $CoFe_2O_4$ nanoparticles (left) and photos of *S*0, *S*100, *S*200, *S*300 samples (right).

Table 1. Structural and magnetic parameters obtained for $CoFe_2O_4$, $CoFe_2O_4$@OA and composites with different degrees of stretching

	D_{XRD}, nm	$\varepsilon\times10^{-3}$	a, Å	H_C, E	M_R/M_S	M_S, emu/g
$CoFe_2O_4$	27.7 ± 0.2	1.59	8.402 ± 0.001	1319	0.358	82
$CoFe_2O_4$@OA				1374	0.370	74
*S*0				1424	0.332	7.7
*S*100				1439	0.380	7.2
*S*200				1493	0.391	7.3
*S*300				1492	0.397	7.0

Note: D_{XRD} is the coherent scattering region, ε is the microstress, a is the lattice constant, H_C is the coercivity, M_R/M_S is the residual magnetization, M_S is the saturation magnetization.

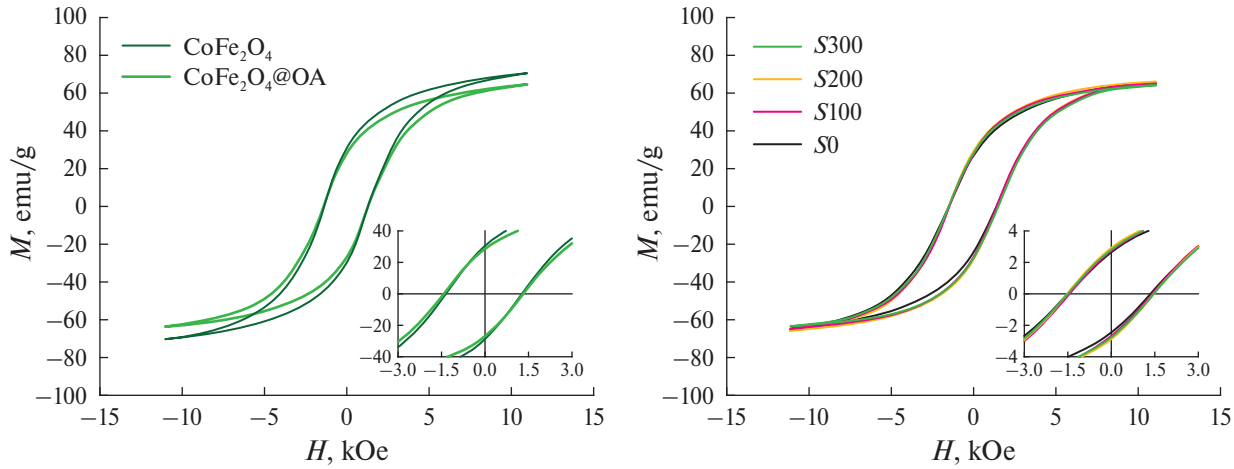

Fig. 2. Field dependence of magnetization for $CoFe_2O_4$ and $CoFe_2O_4$@OA (left) and PVDF– $CoFe_2O_4$@OA at different degrees of stretching (right).

non-interacting single-domain particles according to the Stoner–Wohlfarth model [21].

The observed coercivity H_C for $CoFe_2O_4$ (1319 Oe) is lower than that of OK-coated $CoFe_2O_4$@OA particles (1374 Oe), which reduces particle agglomeration. When $CoFe_2O_4$@OA is incorporated into the composite, a further increase in the coercivity is observed, with H_C increasing with increasing stretching ratio. This mainly indicates a weakening of dipole-dipole interactions between particles, caused by a decrease in agglomeration and an increase in the distance between particles in the matrix [22].

Study of changes in structural properties of composite. X-ray diffraction patterns (XRD) were obtained using a Tongda TD3700 diffractometer equipped with a Co X-ray tube (λ = 1.79 Å). To observe the phase transformations caused by uniaxial deformation of the composite, XRD measurements were carried out in the 2θ angle range from 15º to 35º, where PVDF peaks were observed – α (peaks (020) and (110)) and β (peak (110)) (Fig. 3) [23, 24]. In the XRD pattern of the unstretched PVDF–$CoFe_2O_4$@OA composite, the most pronounced reflections are for the α-phase of PVDF and reflections corresponding to $CoFe_2O_4$ nanoparticles (Fig. 3). The X-ray patterns obtained from stretched composite films show that with an increase in the degree of stretching of the film, a redistribution of peak intensities occurs and, at the same time, a shift to the region of large 2θ angles occurs, which indicates a controlled phase transition from the α- to the β-phase. Observation of the γ-phase from the X-ray pattern is difficult, since the peak from this phase is not expressed and is not resolved due to the α- and β-phases [24].

Fourier transform IR spectroscopy measurements were performed using an FT-801 instrument (SIMEX, Novosibirsk, Russia) in absorption mode with a resolution of 4 cm^{-1}. The obtained IR spectra were used to estimate the quantitative content of α-, β-, and γ-phases in samples with different stretch ratios. The content of individual phases and the total electroactive phase ($F_{EA} = F_\beta + F_\gamma$) were determined using the method proposed in [25].

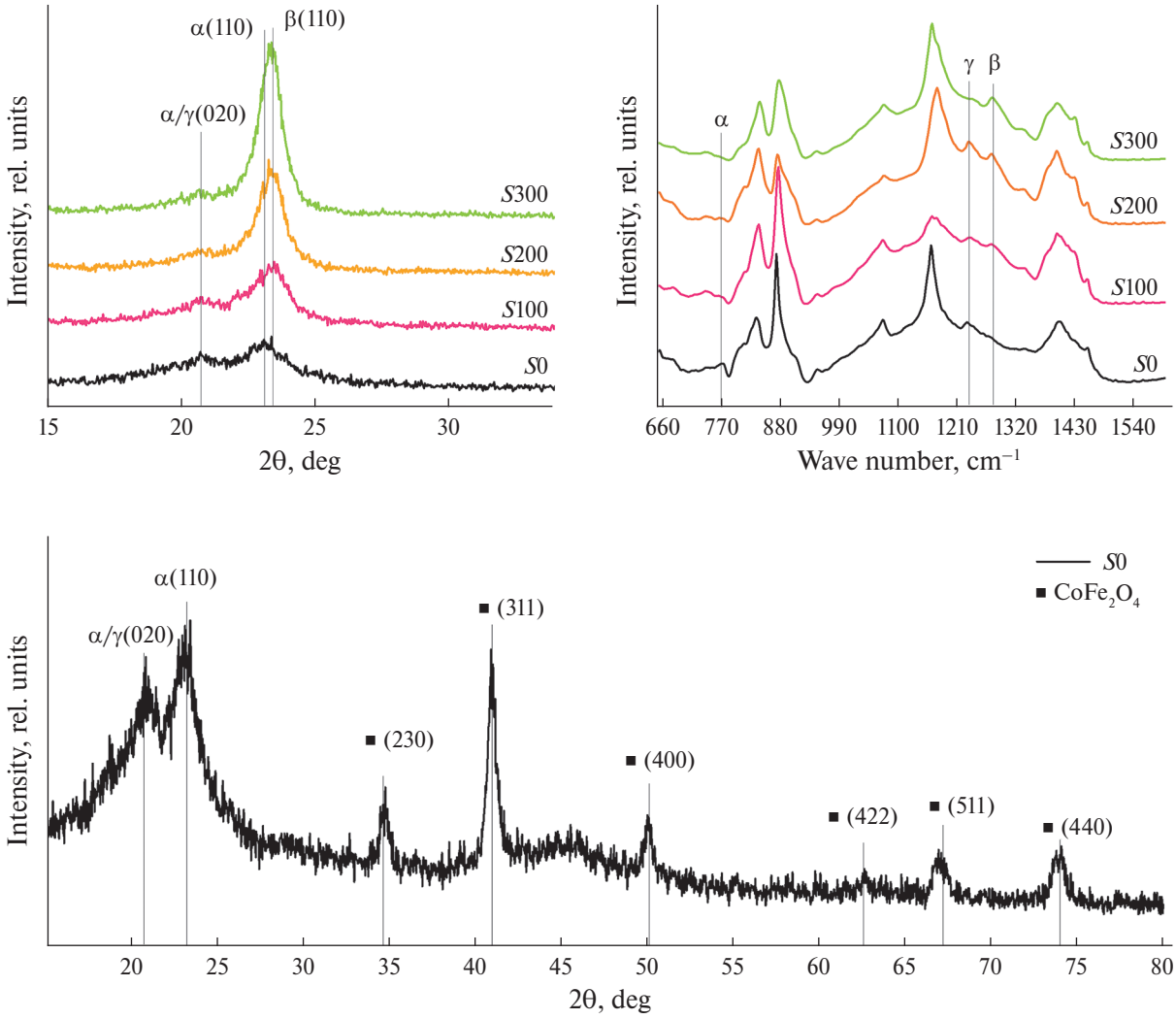

Fig. 3. X-ray diffraction patterns (left) and IR spectra (right) for PVDF– $CoFe_2O_4$@OA composites with different degrees of stretching. X-ray diffraction pattern of unstretched PVDF–CoFe2O4@OA composite (lower graph).

The total electroactive phase was determined by the formula:

$$F_{EA} = \frac{I_{EA}}{\left(\frac{K_{840}}{K_{763}}\right) I_{763} + I_{\mathrm{EA}}} \times 100\%, \qquad (1)$$

where I_{EA} and I_{763} are the absorption coefficients at 840 and 763 cm^{-1} respectively, K_{840} and K_{763} are the absorption coefficients at wave numbers of $7.7 \cdot 10^4$ and $6.1 \cdot 10^4$ cm^2 mol^{-1}, respectively.

To calculate individual electroactive β- and γ-phases, the following formulas were used [25]:

$$F(\beta) = F_{EA}\left(\frac{\Delta H_{\beta'}}{\Delta H_{\beta'} + \Delta H_{\gamma'}}\right) \times 100\%, \qquad (2)$$

$$F(\gamma) = F_{EA}\left(\frac{\Delta H_{\gamma'}}{\Delta H_{\beta'} + \Delta H_{\gamma'}}\right) \times 100\%, \qquad (3)$$

where $\Delta H_{\beta'}$ and $\Delta H_{\gamma'}$ are the height differences (absorption differences) between the peak at about 1275 cm^{-1} and the nearest trough at about 1260 cm^{-1}, and the peak at about 1234 cm^{-1} and the nearest trough at about 1225 cm^{-1}, respectively. The calculated data are presented in Table 2.

The obtained IR spectra (Fig. 3) show that a mixture of α-, β- and γ-phases is formed in all nanocomposites [26]. When stretched, there is a decrease in the intensity of the peaks for the α- and γ-phases (763 and 1234 cm^{-1}, respectively) and an increase in the intensity of the peak around 1275 cm^{-1}, characteristic of the β-phase. The maximum level of the β-phase (91%) is observed at a maximum degree of stretching of 300% compared to the unstretched sample, where the β-phase is equal to 1%. Under the influence of mechanical stress, the γ-phase transforms into the β-phase due to the high similarity of their elementary cells – they are distinguished by a small displacement of transplanar chains along the c-axis, which

Table 2. Calculated from IR spectra α-, β- and γ-phases, electroactive phase F_{EA} (β- + γ-phase), degree of crystallinity χ and melting temperature T_{melt}

Elongation ratio, %	α, %	β, %	γ, %	F_{EA}, %	χ, %*	T_{melt}, °C**
0	26	1	73	74	61	164
100	12	31	57	88	43	162
200	10	39	51	90	45	162
300	8	91	1	92	44	160

Note:*Instrumental error ±3%.
**Instrumental error ±1°C.

occurs during stretching [27], although a parallel process of formation of a mixture of α- and β-phases with subsequent transformation of α- into β-phase is not excluded [28].

The degree of crystallinity of the finished composites was assessed using a differential scanning calorimeter (DSC, NETZSCH 204 F1 Phoenix), comparing the heat of fusion of the sample and fully crystallized PVDF (104.6 J/g) [29]. The samples were analyzed in the range from room temperature to 200°C at a heating rate of 5°C/min in an argon atmosphere. The degree of crystallinity χ was calculated from the equation:

$$\chi = \frac{\Delta H}{H_{100} \cdot \varphi_{PVDF}} \times 100\%, \quad (4)$$

where ΔH is the heat of fusion, H_{100} is the enthalpy for 100% crystalline phase of PVDF, φ_{PVDF} is the mass concentration of PVDF.

When analyzing the DSC curves (Fig. 4), it was found that with an increase in the degree of stretching of the nanocomposite, there is a decrease in the melting temperature (T_{melt}) from 164°C for *S*0 to 160°C for *S*300 (Table 2). Such a temperature shift in the melting peak can be associated with the transition of the system from the γ- to the β-phase or a mixture of the α- and β-phases, since a shift towards lower T_{melt} indicates a decrease in the thickness of the lamellae or spherulites [30, 31], which are associated with the β- and γ-phase, respectively.

Also, when stretching composite films, the content of the crystalline phase decreases by ~16% compared to the unstretched film. Moreover, this decrease is the same for different degrees of stretching, taking into account the measurement error (Table 2). Note that at the lowest stretching coefficient (100%), a change in crystallinity already occurs and does not change further. The literature provides a number of factors that cause changes in crystallinity during stretching: transition to the β-phase and incomplete recrystallization [32]. In this work, the second factor plays the main role, since the degree of crystallinity does not depend on the phase composition of the composite.

Measurement of deformation curves. The deformation curves of the composites studied in the work were obtained using a Microtest 200 N tensile tester (Deben, UK) and are shown in Fig. 5. The tensile strength values for the composites are given in Table 3.

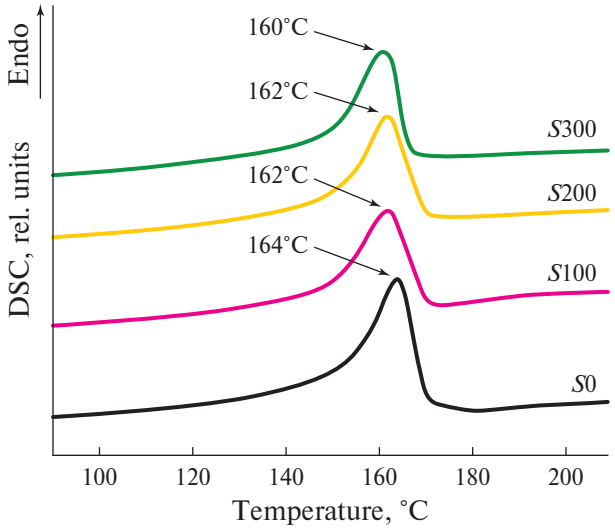

Fig. 4. DSC curves for S0, S100, S200, S300 composites.

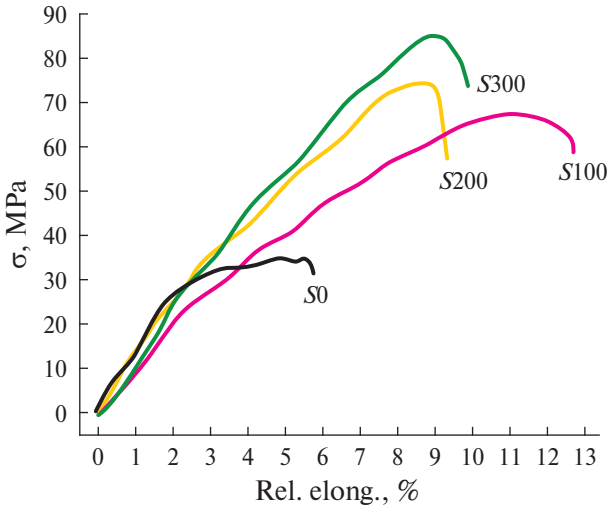

Fig. 5. Stress-strain curves of composites S0, S100, S200, S300.

Table 3. Tensile strength limits for composites *S*0, *S*100, *S*200, *S*300

Elongation ratio, %	Tensile strength, MPa
0	35.7
100	67.9
200	74.5
300	85.0

When stretching composites *S*100, *S*200 and *S*300, an increase in the tensile strength is observed in comparison with the *S*0 sample. This result is explained by the fact that when stretching under the influence of temperature, a simultaneous transition to the β-phase and ordering of its lamellas along the direction of the applied stress occur, which leads to strain hardening of the composite along the selected direction [33]. In this work, it was possible to achieve an increase in the tensile strength by 2.4 times (from 35.7 to 85.0 MPa) when stretching the composite by 300%.

CONCLUSION

The results of the study of the phase transformation process by uniaxial stretching of a PVDF-based composite with the addition of 10 wt.% cobalt ferrite $CoFe_2O_4$ MNP coated with oleic acid are presented.

The PVDF–$CoFe_2O_4$@OA composite films were stretched at 100°C by 100, 200, and 300%. A controlled transition from a mixture of the α- and γ-phases to the β-phase was observed. This transition was noted both in the X-ray diffraction patterns, where a redistribution of the reflex intensities occurred, and in the IR spectra. Recalculation to numerical values based on the intensities of the peaks at 763, 1234, and 1275 cm^{-1} showed an increase in the amount of the β-phase from 1% for the unstretched composite to 91% for the composite stretched by 300%. The content of the electroactive phase increased from 74 to 92%. The results of differential scanning calorimetry measurements also showed a controlled transition to the β-phase, which is evident from the shift in the temperature of the endothermic melting peak from 164 to 160°C. Thus, when the composite is stretched by 300%, the maximum transition from the α- and γ-phases to the β-phase occurs, which makes it possible to develop more efficient magnetoelectric materials.

The phase changes in the composite affected the changes in mechanical properties. Under uniaxial tension of PVDF–$CoFe_2O_4$@OA composites, the ultimate strength increased from 5.7 to 85.0 MPa due to the induction of uniaxial anisotropy. This type of tension also affects the magnetic properties. Under tension, HC gradually increases due to a decrease in dipole–dipole interactions due to an increase in the distance between particles.

It should also be noted that when stretched, the mechanical properties of the composite change significantly, which is especially important for applications in regenerative medicine, since the developed composite can be used as a substrate for cell growth with their subsequent stimulation by means of an external magnetic field.

FUNDING

The study was carried out with financial support from the Russian Science Foundation (project No. 21-72-30032).

CONFLICT OF INTERESTS

The authors declare that they have no known competing financial interests or personal relationships that could have influence on the work reported in this paper.

REFERENCES

1. *Saxena P., Shukla P.* // Adv. Compos. Hybrid Mater. 2021. V. 4. P. 8. https://doi.org/10.1007/s42114-021-00217-0
2. *Dallaev R., Pisarenko T., Sobola D. et al.* // Polymers (Basel). 2022. V. 14. No. 22. P. 1. https://doi.org/10.3390/polym14224793
3. *Su Y.P., Sim L.N., Li X. et al.* // J. Memb. Sci. 2021. V. 620. P. 118818. https://doi.org/10.1016/j.memsci.2020.118818
4. *Bichurin M., Petrov R., Sokolov O. et al.* // Sensors. 2021. V. 21. No. 18. P. 6232. https://doi.org/10.3390/s21186232
5. *Narita F., Fox M.* // Adv. Eng. Mater. 2018. V. 20. No. 5. P. 1. https://doi.org/10.1002/adem.201700743
6. *Alibakhshi H., Esfahani H., Sharifi E.* // Ceram. Int. 2024. V. 50. No. 5. P. 8017. https://linkinghub.elsevier.com/retrieve/pii/S0272884223040506
7. *Liu F., Hashim N.A., Liu Y., Abed R.* // J. Memb. Sci. 2011. V. 375. No. 1–2. P. 1. http://dx.doi.org/10.1016/j.memsci.2011.03.014
8. *Lovinger A.J.* // Science. 1983. V. 220. No. 4602. P. 1115. https://doi.org/10.1126/science.220.4602.1115
9. *Pereira N., Lima A., Lanceros-Mendez S., Martins P.* // Materials. 2020. V. 13. No. 18. P. 4033. https://doi.org/10.3390/ma13184033
10. *Omelyanchik A., Antipova V., Gritsenko Ch. et al.* // Nanomaterials. 2021. V. 11. No. 5. P. 1154. https://doi.org/10.3390/nano11051154
11. *Antipova V., Omelyanchik A., Sobolev K. et al.* // Nanobiotechnology Reports. 2023. V. 18. Suppl. 1. P. S186. https://doi.org/10.1134/S2635167623600967

12. *Koç M., Demirci C., Parali L. et al.* // J. Mater. Sci. Mater. Electron. 2022. V. 33. No. 10. P. 8048. https://doi.org/10.1007/s10854-022-07956-w
13. *Cozza E.S., Monticelli O., Marsano E., Cebe P.* // Polym. Int. 2013. V. 62. No. 1. P. 41. http://dx.doi.org/10.1002/pi.4314
14. *Sharma M., Madras G., Bose S.* // Phys. Chem. Chem. Phys. 2014. V. 16. No. 28. P. 14792. http://dx.doi.org/10.1039/c4cp01004c
15. *Chen B., Yuan M., Ma R. et al.* // Chem. Eng. J. 2022. V. 433. P. 134475. http://dx.doi.org/10.1016/j.cej.2021.134475
16. J*ovanović S., Spreitzer M., Otoničar M. et al.* // J. Alloys Compd. 2014. V. 589. P. 271. http://dx.doi.org/10.1016/j.jallcom.2013.11.217
17. *Botvin V., Fetisova A., Mukhortova Y. et al.* // Polymers. 2023. V. 15. No. 14. P. 3135. http://dx.doi.org/10.3390/polym15143135
18. *Terzić I., Meereboer N.L., Mellema H.H. et al.* // J. Mater. Chem. C. 2019. V. 7. No. 4. P. 968. https://doi.org/10.1039/C8TC05017A
19. *Ribeiro C., Costa C., Correia D. et al.* // Nat. Protoc. 2018. V. 13. No. 4. P. 681. http://dx.doi.org/10.1038/nprot.2017.157
20. *Sayyar S., Aslibeiki B., Asgari A.* // Phys. Appl. Mater. 2022. V. 2. P. 165. https://doi.org/10.22075/ppam.2022.29079.1047
21. *Stoner B., Wohlfarth P.A.* // Phys. Dep. 1948. V. 250. No. 826. P. 599. http://dx.doi.org/10.1098/rsta.1948.0007
22. *Salnikov V.D., Aga-Tagieva S., Kolesnikova V. et al.* // J. Magn. Magn. Mater. 2024. V. 595. P. 171498. http://dx.doi.org/10.1016/j.jmmm.2023.171498
23. *Zhang L., Li S., Zhu Z. et al.* // Adv. Funct. Mater. 2023. V. 33. No. 38. P. 2301302. http://dx.doi.org/10.1002/adfm.202301302
24. *Satapathy S., Pawar S., Gupta P.K., Varma K.* // Bull. Mater. Sci. 2011. V. 34. No. 4. P. 727. http://dx.doi.org/10.1007/s12034-011-0187-0
25. *Cai X., Lei T., Sun D., Lin L.* // RSC Adv. 2017. V. 7. No. 25. P. 15382. http://dx.doi.org/10.1039/C7RA01267E
26. *Peters A., Candau S.J.* // Macromolecules. 1986. V. 19. P. 1952. https://doi.org/10.1021/ma00161a029
27. Developments in Crystalline Polymers – 1. / Ed. Bassett D.C. Dordrecht: Springer, 1982. 279 p. https://doi.org/10.1007/978-94-009-7343-5
28. *Salimi A., Yousefi A.A.* // J. Polym. Sci. B. Polym. Phys. 2004. V. 42. No. 18. P. 3487. http://dx.doi.org/10.1002/polb.20223
29. *Orudzhev F., Ramazanov S., Sobola D. et al.* // Nano Energy. 2021. V. 90 (B). P. 106586. http://dx.doi.org/10.1016/j.nanoen.2021.106586
30. *Silva M.P., Costa C.M., Sencadas V. et al.* // J. Polym. Res. 2011. V. 18. No. 6. P. 1451. http://dx.doi.org/10.1007/s10965-010-9550-x
31. *Keshmirizadeh E., Modarress H., Eliassi A., Mansoori G.A.* // Eur. Polym. J. 2003. V. 39. No. 6. P. 1141. http://dx.doi.org/10.1016/S0014-3057(02)00373-7
32. *Miri V., Persyn O., Seguela R., Lefebvre J.M.* // Eur. Polym. J. 2011. V. 47. No. 1. P. 88. http://dx.doi.org/10.1016/j.eurpolymj.2010.09.006
33. *Zhou Y., Liu W., Tan B. et al.* // Polymers. 2021. V. 13. No. 7. P. 998. http://dx.doi.org/10.3390/polym13070998